processes

MDPI

Article

Spray Structure and Characteristics of a Pressure-Swirl Dust Suppression Nozzle Using a Phase Doppler Particle Analyze

Junpeng Wang, Cuicui Xu *, Gang Zhou and Yansong Zhang

Safety Engineering Department, College of Safety and Environmental Engineering, Shandong University of Science and Technology, Qingdao 266590, China; wjp0070@163.com (J.W.); zhougang@sdust.edu.cn (G.Z.); zys6407@163.com (Y.Z.)

* Correspondence: xucuicui519@163.com; Tel.: +86-0532-8605-7748

Received: 10 July 2020; Accepted: 28 August 2020; Published: 10 September 2020

Abstract: In order to understand the characteristics of the spray field of a dust suppression nozzle and provide a reference for dust nozzle selection according to dust characteristics, a three-dimensional phase Doppler particle analyzer (PDPA) spray measurement system is used to analyze the droplet size and velocity characteristics in a spray field, particularly the joint particle size–velocity distribution. According to the results, after the ejection of the jet from the nozzle, the droplets initially maintained some velocity; however, the distribution of particles with different sizes was not uniform. As the spray distance increased, the droplet velocity decreased significantly, and the particle size distribution changed very little. As the distance increased further, the large droplets separated into smaller droplets, and their velocity decreased rapidly. The distributions of the particle size and velocity of the droplets then became stable. Based on the particle size-velocity distribution characteristics, the spray structure of pressure-swirl nozzles can be divided into five regions, i.e., the mixing, expansion, stabilization, decay, and rarefied regions. The expansion, stabilization, and decay regions are the effective dust fall areas. In addition, the droplet size in the stabilization region is the most uniform, indicating that this region is the best dust fall region. The conclusions can provide abundant calibration data for spray dust fall nozzles.

Keywords: pressure-swirl nozzle; PDPA; joint particle size–velocity distribution; spray structure; dust fall

1. Introduction

With the development of efficient mechanization, the amount of coal mine dust is also increasing. The high concentration of dust on the production site is very harmful, as it not only brings harm to the physical and mental health of underground workers, but also threatens the production safety of coal mines. Every year, explosion accidents and pneumoconiosis caused by high dust content in the working environment have brought huge economic losses to the country. Therefore, the research on dust control has important theoretical significance and social value for improving the occupational safety of miners and ensuring production safety in an underground mine. Spray-based dust-settling technology is the most widely used and effective dust control measure in coal mines [1–3]. When using a spray, the eventual success with regard to dust suppression depends on multiple factors, including inertial impaction, gravity settling, Brownian diffusion, interception, and electrostatic collection [4–9]. In 1973, an American scholar, Cheng [10], proposed a theoretical equation for the collection of airborne dust by a water spray, which first promoted the study of "water spray theory". Charinpanitkul et al. [11] simulated the dust removal effects of different water mist particle sizes on dust with different particle sizes and proposed that the maximal dust removal efficiency was also confirmed

by water droplets with smaller size and narrower size distribution. The nozzle is a key component of the spray dust-control system, and its atomization capability directly impacts the practical dust suppression effect. When water is ejected from the nozzle, the distribution of the water velocity will affect the droplet's breakup process and thus affect the size distributions of droplets in the spray field. Smaller droplets at a greater velocity relative to airflow display a high dust-collision and dust-capture efficiency [12–17]. Therefore, it is vital that we investigate atomization of the nozzle to enhance the efficiency of dust-suppression sprays.

The existing research shows that the droplet size in a spray field is an important index to evaluate whether the droplet can effectively reduce dust [18–21]. There are many methods to measure the droplet size in a spray field, such as the shadowgraph method and the schlieren method. With the development of optical technology, new optical measurement technologies have been applied, which have greatly advanced research into droplet size. At present, the mainstream testing methods include the Malvern laser particle size analysis, laser Doppler velocimetry, phase Doppler particle analysis, and particle image velocimetry. For example, Zhou et al. [19] used the Malvern laser particle size analyzer to conduct tests involving the atomization particle size under various pressures. They found that the droplet size is the smallest at the center of the spray field and gradually increases towards the edge. For the same nozzle at different pressures, the change of the atomization particle size of a large-diameter nozzle is not obvious, but that of small diameter nozzle is obvious. Pollock et al. [22] used a phase Doppler particle analyzer (PDPA) to investigate water droplet size and velocity characteristics for hollow-cone, full-cone, flat-fan, and air-atomizing spray nozzles at similar operating parameters. Test results indicated that the hollow-cone nozzles, especially the wider-angle nozzle, tend to generate smaller and slower velocity droplets, while the flat-fan nozzles tend to generate larger droplet sizes at moderate velocities. On the other hand, the full-cone (water-only and air-atomizing) nozzles tend to generate droplet sizes in a range between those of the hollow-cone and flat-fan spray nozzles, with noticeably higher mean droplet velocities generated from the air-atomizing sprays.

According to the above results, research on dust suppression nozzles has mainly been focused on the effect of spray pressure and nozzle types. The spatial distribution of droplets has been limited to the change in the central axis. There has been no analysis of droplet characteristics in the whole spray field. Therefore, it is necessary to further study the spatial factors affecting the dust fall efficiency. In this study, we used a three-dimensional (3-D) PDPA spray measurement system to analyze the distributions of different droplet sizes and velocities in the spray field, particularly the joint particle size–velocity distribution, to fully understand the spatial movements of droplets as the spray distance increases and provide a large amount of calibration data for spray structure. Through this paper, we can further understand the characteristics of the droplets in the spray field of the dust nozzle and provide a reference for dust nozzle selection according to dust characteristics.

2. Experimental Setup and Procedure

2.1. Test Nozzle Specification

Pressure nozzles are widely used in response to high dust concentrations in mining and excavation [23–25]. Pressure-swirl nozzles are the most widely used type of atomizing nozzle in underground coal mines. Therefore, a pressure-swirl nozzle was selected as the research object of this study, and its atomization characteristics were studied in depth. Figure 1 presents a schematic view of the pressure-type nozzle, and Table 1 shows its specific geometric parameters.

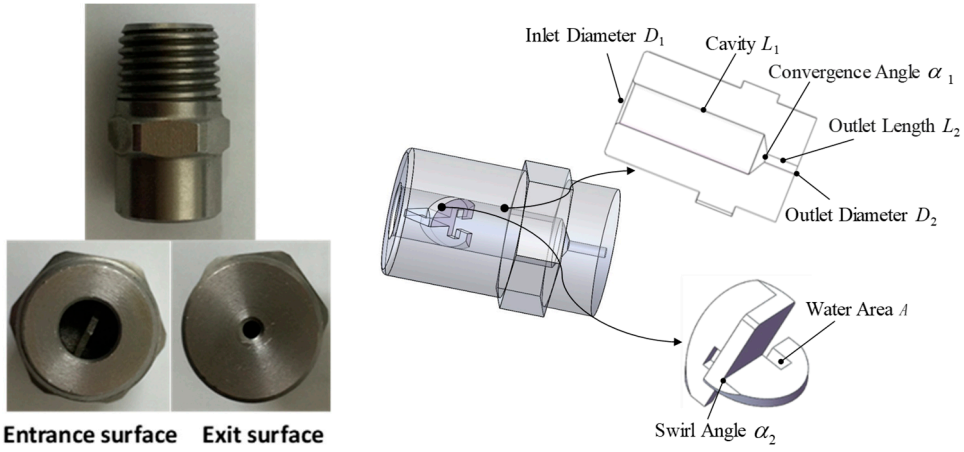

(**a**) Physical picture (**b**) Internal structure

Figure 1. Distributor pressure nozzle.

Table 1. Structural parameters of the nozzle.

L_1(mm)	D_1(mm)	α_1(°)	D_2(mm)	L_2(mm)	A (mm^2)	α_2(°)
5	15	100	1.5	6	1	35

2.2. Experimental Setup and Measurement Technique

2.2.1. Experimental System

All experiments were conducted using an atomizing test system based on a PDPA. Figure 2 shows a schematic diagram of the atomizing test system, which consisted of an atomizing control system and a PDPA system. The atomizing control system is comprised of a water tank, pressure gauge, high-pressure water pump, and so on.

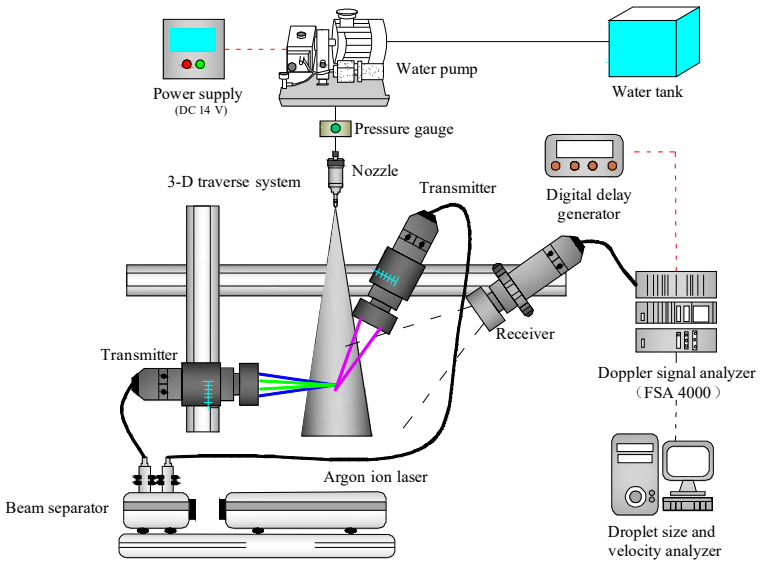

Figure 2. Schematic diagram of the atomizing test system.

A PDPA (Dantec) system was used to analyze the droplet size and velocity, as shown in Figure 3. The monochromatic light ray from the laser was split by a beam separator into six beams in three different colors, i.e., green (514.5 nm), blue (488.0 nm), and violet (476.5 nm), and then sent to

the transmitters. We used the Flowsizer software to analyze the droplet velocity and particle size distributions. The transmitters and receivers were fixed to a 3-D traverse system with a pitch of 0.1 mm. The data could be quickly and automatically collected, and information about the whole spray field could be obtained by controlling the traverse system. Table 2 shows the main parameters of the PDPA.

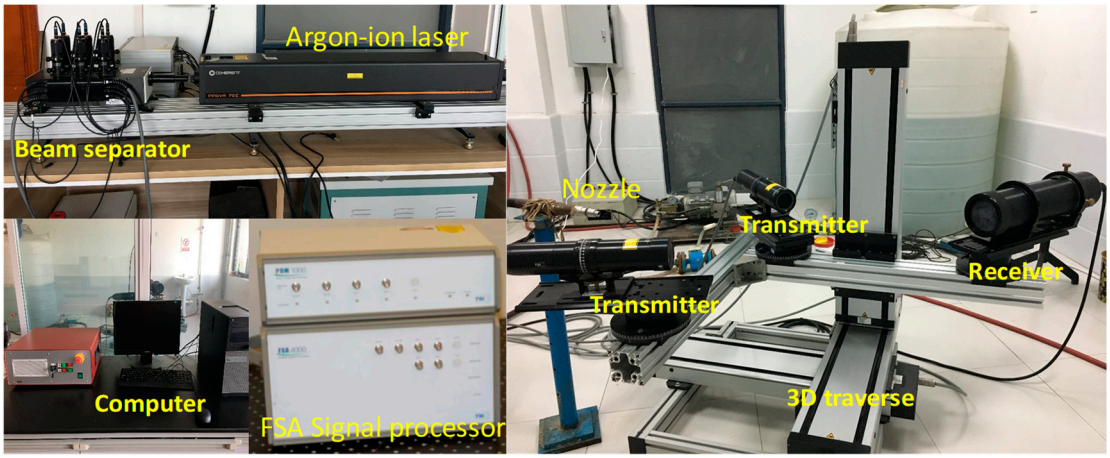

Figure 3. Installed phase Doppler particle analyzer (PDPA) system.

Table 2. Optical setup and run settings of the PDPA system.

Parameters	Value
Bragg cell frequency	40 MHz
Focal length of transmitting probe	750 mm
Beam diameter	1.77 mm
Beam spacing	50 mm
Scattering angle	40°
Velocity measurement range	−313 to 1600 m/s
Diameter measurement range	0.5 to 5000 μm
Band pass filter	1–10 MHz
Burst threshold	30–300 mV

2.2.2. Error Analysis

PDPA measurement system itself has some measurement error. The Doppler frequency obtained in the measurement has a width and is not a single frequency. This broadening phenomenon will cause measurement error. There are many reasons for the broadening, such as the finite transit time of the scattering particles in the measurement body, the velocity gradient, and Brownian motion of particles in the velocity field. The error caused by frequency broadening can be suppressed by setting system parameters to match the measured flow field. Taking account of the above errors, the uncertainties in the PDPA measurement of drop velocity and size are estimated to be 1% and 3%, respectively.

The measured values were statistically average. For each measurement point, we ceased sampling when either of the following conditions was satisfied: (1) the effective sample size reached 2000 or (2) the measurement took 15 s. Panão and his co-workers [26] also determined that if the measurements stop at a sample size of 1000 drops, any mean diameter calculated would only be 1% higher than the value calculated if more than 3000 samples were acquired to describe the spray at that measurement point.

2.3. Testing and Analytical Methods

When we measured the spray using the PDPA, the nozzle was arranged into a rack to eject horizontally and parallel to the X-axis of the traverse system. Therefore, the spray was ejected in the X-direction. In the following experimental analysis, we obtained the axial distribution from the center of a cross-section at a distance of X from the nozzle. The radial distribution was obtained from

this cross-section at a measurement point with a distance of Y from the center of the nozzle, and the tangential distribution was obtained from this cross-section at a measurement point with a distance of Z from the center of the nozzle. The three light beams could not meet at the exit as they were blocked by the nozzle. Therefore, no valid data could be obtained at the exit. Thus, we set the first measurement point to be 50 mm from the nozzle, and we set the step size to 50 mm. The step size in the radial direction (Y) was also set to 50 mm. The spray was ejected horizontally during measurement. At greater distances, droplets near the edge of the spray field were scattered onto the transmitter and receiver lenses of the PDPA system, preventing measurement. Therefore, we took X up to 1000 mm. Within this range, the spray remained in a good condition and droplets near the boundary did not contaminate the lenses, ensuring successful measurement.

The flow sizer software can display the experimental statistical results in real time, as shown in Figure 4. The first chart shows the SMD (Sauter mean diameter) of the droplet at the measurement point, and the statistical results of D10, D20, D30, D32 and D43 are shown in diameter statistics. The remaining charts show the average velocity distribution characteristics of the droplets at the measurement points. Green light (ch.1) represents tangential velocity (Z-axis velocity), blue light (ch.2) represents radial velocity (Y-axis velocity), and purple light (ch.3) represents axial velocity (X-axis velocity).

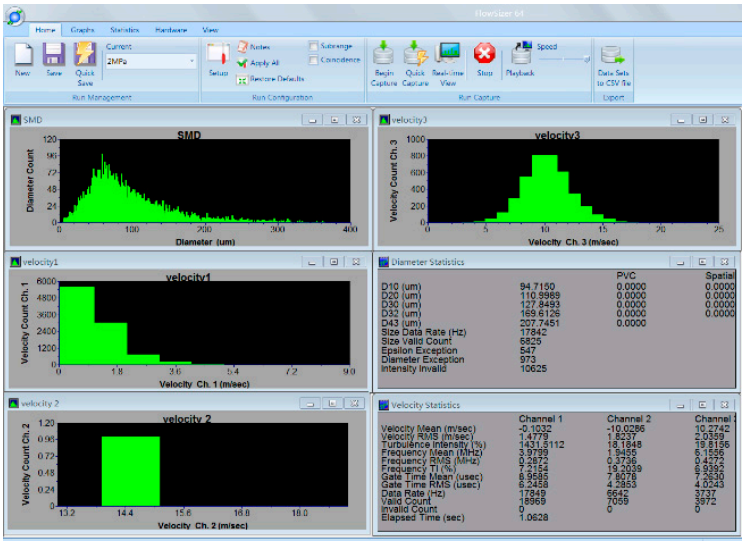

Figure 4. Flowsizer software display interface.

The specifications of the test nozzle are provided in Section 2.1. We selected an initial pressure of 2 MPa and changed the pressure to 3, 4, and 5 MPa. Before testing, we photographed the spray using high-speed cameras, and, based on the captured spray angle, we determined the number of measurement points (see Figure 5). Owing to the axial symmetry of the spray and to conserve time, we only collected statistics on one side.

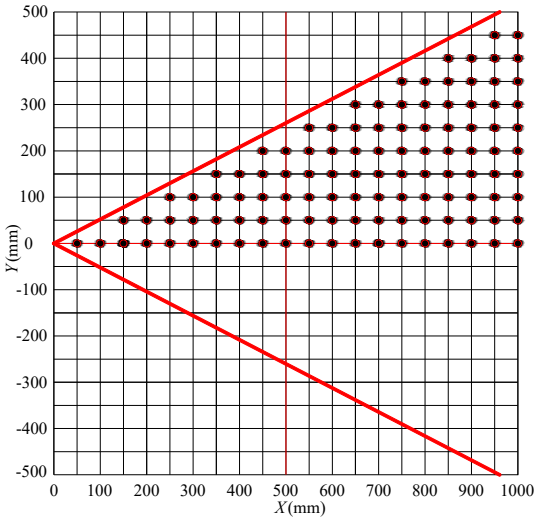

Figure 5. Measuring point layout.

3. Results and Discussion

3.1. Droplet Size

3.1.1. Characteristics of Particles in the Axial Direction

The capture of dust by a droplet is the result of the interaction events occurring between surfaces. D_{32}, as the area-weighted mean diameter, is most suitable for monitoring the proportion of fine particles present. Thus, the SMD (D_{32}) was selected to illustrate the mean droplet diameter in atomization investigations [27–29]. Y was taken up to 200 mm to ensure that enough measurement points were used for analysis. Figure 6 shows the comparison curves of the SMD distribution along the axial direction (X-direction).

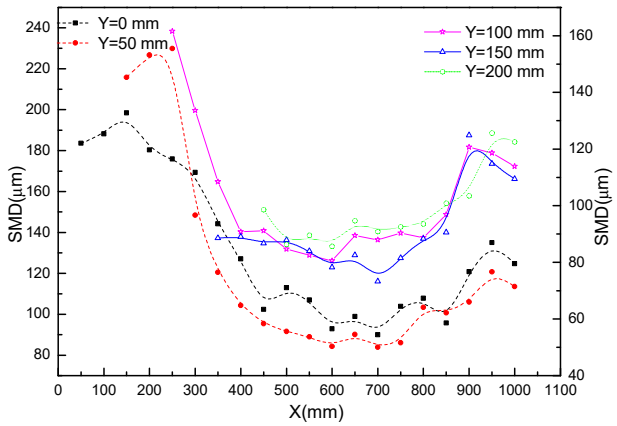

Figure 6. Comparison curves of the SMD distribution along the axial direction.

As the distance in the axial direction increased, several stages of regular variations in the SMD occurred. At Y = 0 mm, the SMD curve underwent approximately four stages of changes: (1) When X = 50–150 mm, the SMD increased as X increased. This is likely due to the concentration of the droplets just after leaving the nozzle [30]. During sampling, strong droplet coalescence occurred due to incomplete atomization. (2) When X = 150–450 mm, the SMD decreased rapidly by up to 48.4%. This indicates that the splitting of single droplets was predominant during this stage. (3) When X = 450–800, the SMD fluctuated between 90 and 110 μm. This indicates that the droplets were stable under both internal and external forces and that the SMD reached a uniform distribution.

(4) When X = 800–1000 mm, the fluctuations in SMD were greater, as the amplitude increased by 16%. This suggests that droplet collisions and coalescences became predominant. As shown in Figure 6, the variation in SMD when Y = 50 mm was similar to that when Y = 0 mm. With an increase in the distance, the SMD increased, indicating an increase in the area in which concentrated droplets were concentrated. The SMD only began to decrease significantly at X = 300 mm, and it varied between 80 and 95 μm when X = 450 mm. The droplet collision and coalescence rates began to increase when X = 850 mm. When Y = 100 mm, the curve began to change. The SMD did not initially increase with X. This indicated that the droplets were directly entering the fast breakup phase.

When Y = 150 mm, the SMD initially mildly oscillated but then gradually increased. The SMD reached the minimum value of 73.25 μm when X = 700 mm. It then increased by 49.4% at X = 1000 mm. At Y = 200 mm, which was close to the edge of the spray field, the SMD experienced more pronounced oscillations but was similar to the behavior at Y = 150 mm.

3.1.2. Characteristics of Particles in the Radial Direction

To further investigate the variations in SMD at each cross-section, we analyzed the SMD in the radial direction. According to our analysis in Section 3.1.1, stage-wise changes in SMD were observed in the axial direction. Therefore, we selected several typical cross-sections for study based on the characteristics in each region. These cross-sections were located at X = 100, 200, 450, and 800 mm. With a step size of 50 mm, the cross-section close to the nozzle would only be able to contain one measurement point. Therefore, for particle size analysis, we set the step size to 20 mm to ensure sufficient data collection. Figure 7 shows the SMD distribution along the radial direction in the four selected cross-sections.

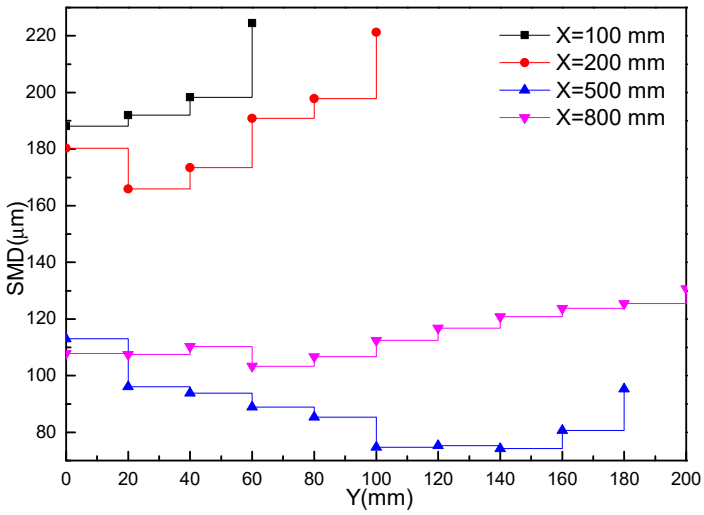

Figure 7. Comparison curve of the axial velocity along the axial direction.

As shown in Figure 7, when X = 100 mm, the droplet radius increased from the center to the edge of the spray field. This is due to the great droplet density, indicating that some droplets were overlapping. In the other cross-sections (X = 200, 450, and 800 mm), the SMD changed in the radial direction and exhibited similar behavior, i.e., it first decreased and then increased. This indicates that the droplets initially separate into smaller droplets as they spread outward from the center. Then, with an increase in Y, the SMD increased for the following two reasons: First, the droplets extensively exchanged energy with the environment, and the loss of kinetic energy increased with the radial distance. Under the impact of the atmosphere, inelastic collisions caused the SMD to increase. Second, larger droplets exhibited higher inertia and smaller air resistance per unit volume, allowing them to travel farther. Furthermore, the small droplets near the edge of the spray field evaporated quickly, hindering measurement.

3.2. Droplet Velocity

3.2.1. Characteristics of Velocity in the Axial Direction

The velocity in the axial direction represents the kinetic energy required for the droplets to move forward. A greater velocity in the axial direction means that the droplets possess higher energy to move forward [31]. Figure 8 shows the regularity of the distribution of the axial velocity in the axial direction. As the spray distance increased, the axial velocity decreased, but this decrease slowed gradually. The main reason for this decrease was that the nearby spray was required to overcome the air shear resistance to move forward. Along the axial direction of the spray (Y = 0 mm), the axial velocity decreased significantly from near the nozzle's exit to X = 500 mm. Over this distance, the velocity of the droplets decreased by up to 51.3%. Along the line Y = 50 mm parallel to the axial direction, there was still a clear decrease, which reached 51.9% at X = 500 mm. When Y was between 100 and 150 mm, as the axial distance increased, the decrease in the axial velocity slowed. Along the line of Y = 200 mm parallel to the spray, the axial velocity remained almost the same, maintaining a value between 1 and 4 m/s. The axial velocity decreased further from the axial direction (Y = 0 mm), but became more stable. It can be speculated that the outer region of the spray field tended to stabilize, but the forward momentum diminished.

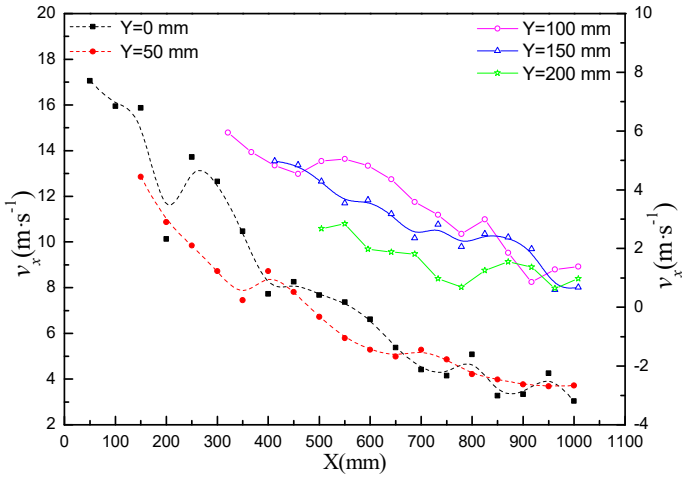

Figure 8. Comparison curve of the radial velocity along the axial direction.

The velocity in the radial direction represents the kinetic energy used for the droplets to expand. A higher velocity indicates that the droplets are more likely to move outward [32]. As shown in Figure 9, the radial velocity exhibits a similar scale to the axial velocity but is 50–60% smaller. This suggests that the swirl structure of the nozzle greatly enhanced the radial velocity. Along the axial line of the spray (Y = 0 mm), with an increase in the distance, the radial velocity first increased gradually and then decreased. The increase reached 41.5% at X = 150 mm, after which the velocity first decreased rapidly but then decreased more slowly. The decrease reached 58.2% at X = 500 mm; beyond this, the radial velocity was very small, between 0–3 m/s. When Y = 50 mm and Y = 100 mm, the behaviors were consistent with those at Y = 0 mm, although with the initial increase in the radial velocity were 9.5% and 4.9% slower, respectively. When Y = 150 mm and Y = 200 mm, the radial velocity decreased throughout the spray, indicating a constant weakening in its expansion.

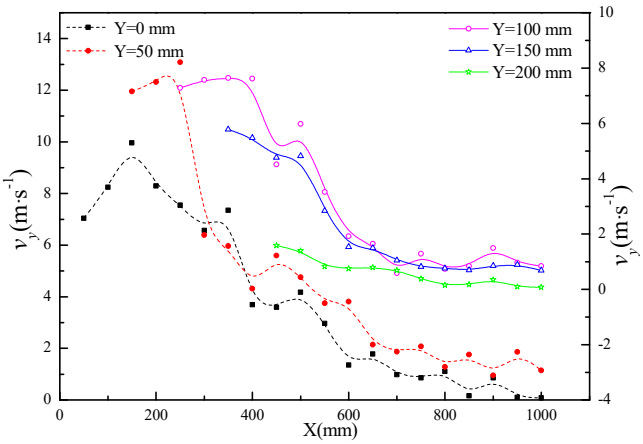

Figure 9. Comparison curve of the radial velocity along the axial direction.

3.2.2. Characteristics of Velocity in the Radial Direction

Along with the velocity changes along the radial direction, the changes in the radial direction within each cross-section are also very important in the formation of the spray field. Therefore, it is necessary to study the variations in the velocity radially in the cross-section. Here, we focused on the changes in the axial and radial velocities using the representative cross-sections used in Section 3.1.2 as our object of study. For details, see Figures 10 and 11.

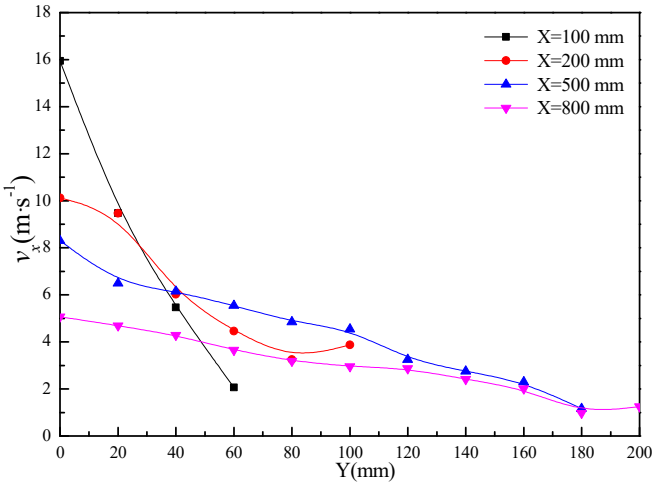

Figure 10. Comparison curve of the axial velocity along the radial direction.

As shown in Figure 10, the radial velocity decreased gradually in the radial direction and slowly approached 0 at the edge of the spray field. This indicates that the ejector pumping capability of the axial velocity declined gradually towards the edge of the spray field. The extent of decrease in the radial velocity with increasing spray distance was distinct for each cross-section: at the cross-sections with X = 100 mm and X = 200 mm, the decline in axial velocity was approximately parabolic; at X = 450 mm, the decline was almost linear; and, after X = 800 mm, the axial velocity changed very slightly, unlike that in the previous cross-sections. According to this analysis, the droplets lost momentum as the spray distance increased, gradually shifting from internal-force to external-force dominance. When the axial velocity decreased by such an amount that resulted in a balance between the internal and external forces on the droplets, the droplets tended to stop moving forward.

As shown in Figure 11, with an increase in the spray distance, the changes in the radial velocity differed between different cross-sections. When X = 100 mm and X = 200 mm, the radial velocities increased by 68.4% and 85.7%, respectively. Therefore, the spray expands rapidly during this interval.

This was maintained until X = 450 mm, where the increase was 67.9%. This indicated that the spray was still expanding at this distance, though at a lower rate. At Y = 800 mm, the radial velocity remained between 0 and 1 m/s. At this point, the expansion was solely maintained by the inertia of the droplets. Although it was compressed by air in the atmosphere, the spray field continued to expand for some distance due to inertia. However, the radial velocity was very small, limiting the space available for expansion. The expansion rate at X = 100 mm was significantly higher than that of the following cross-sections, and the radial velocity in the final cross-section was one order of magnitude lower than that at X = 100 mm. This indicates that, near the nozzle's exit, the spray is locally concentrated in a small region and has high expansion energy. However, after some distance, the spray gradually dissipates and loses expansion energy.

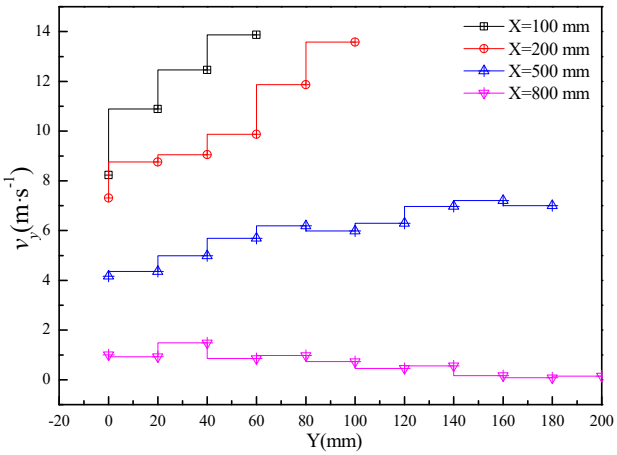

Figure 11. Comparison curve of the radial velocity along the radial direction.

3.3. *Characteristics of the Droplets' Joint Particle Size–Velocity Distribution*

According to jet atomization theories, the particle size distribution is closely related to the velocity distribution during spraying [33]. The velocity of the droplets directly impacts their breakup, thereby affecting the eventual distribution of the particle sizes in the spray field. Therefore, in this section, we consider the particle size and velocity distributions jointly to elucidate the spray's dynamics during its development.

Figure 12 presents a joint particle size–velocity distribution scatter plot at different locations with an injection pressure of 2 MPa. In the region near the nozzle (X = 50 mm), both the axial and radial velocities were highly dispersed, increasing the likelihood of smaller droplets having a higher axial velocity. When X = 100 mm, the droplets' axial velocity decreased significantly, but the radial velocity increased greatly, resulting in a concentrated distribution. By comparing Figures 12a and 12b, it can be seen that the difference in the velocity between droplets with different particle sizes decreased. This indicated that, with the development of the spray, the velocity of droplets with small radii decreased significantly, while larger droplets maintained a high speed. When X = 200 mm, the axial velocity of the droplets still decreased significantly, while the radial velocity did not change greatly. When X = 450 mm, the axial velocity decreased slightly, while the radial velocity decreased significantly. By X = 600 mm, the average velocity of the droplets had decreased by 70%. By comparing Figure 12c, Figure 12d, and Figure 12e, it can be seen that the number of smaller droplets increased, while the number of larger droplets decreased but could better maintain a stable velocity. The droplets gradually began to stratify in the spray field. At X = 600 mm, the velocity of the small droplets was very small, while that of the larger droplets was significantly higher. It can be speculated that, during spraying, small droplets interact with the surrounding air and gradually lose momentum. Meanwhile, large droplets separated into smaller droplets. The rapid atomization process stabilized slowly as the spray developed. As shown in the velocity scatter plot when X = 800 mm (Figure 12f), the number of large

droplets increased significantly, but their velocity remained low. This indicated that these large droplets were formed by the coalescence of smaller droplets.

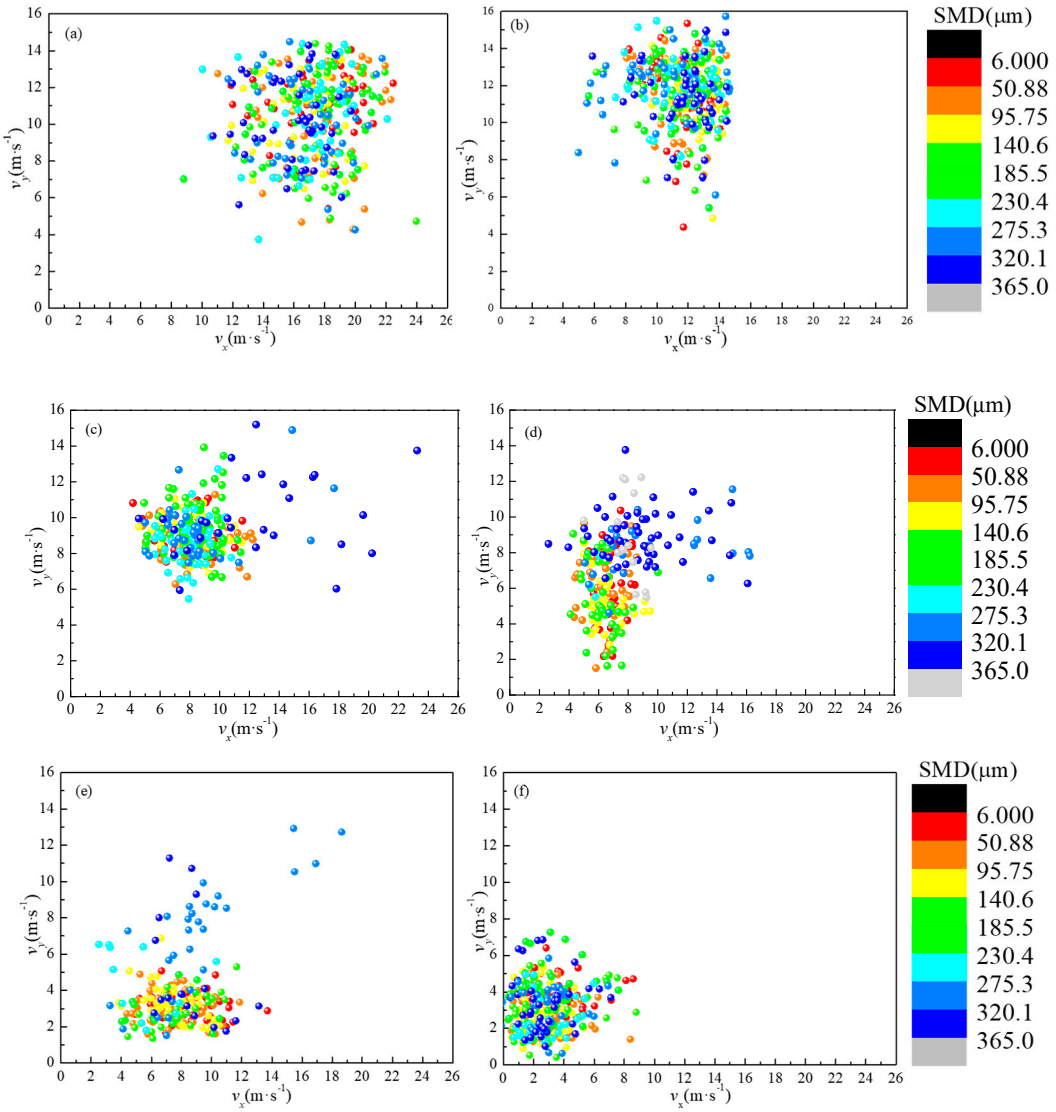

Figure 12. Joint particle size–velocity distribution scatter plot: (**a**) X = 50 mm, (**b**) X = 100 mm, (**c**) X = 200 mm, (**d**) X = 450 mm, (**e**) X = 600 mm, and (**f**) X = 800 mm.

From the descriptions above, the development of the spray field can be summarized as follows. After the ejection of the jet from the nozzle, the droplets initially maintained some velocity, but the distribution of particles with different sizes was not uniform. As the spray distance increased, the droplet velocity decreased significantly, and the particle size distribution changed very little. As the distance increased further, the large droplets separated into smaller droplets, increasing their number accordingly, but their velocity decreased rapidly. However, the large droplets that did not break up, or did not sufficiently break up, maintained their high velocity. The low-speed small droplets then collided, producing larger droplets with low speeds. The droplets that did not sufficiently break up continued to separate. At this point, the distributions of the particle size and velocity of the droplets stabilized. As the spray distance increased further, the droplet velocity decreased significantly and the small droplets coalesced, thus increasing the number of large droplets.

3.4. Spray Structure of the Pressure-Swirl Nozzle

In Section 3.3, we used our analysis of the joint particle size–velocity distribution to microscopically elucidate the spray development process. However, for engineering applications, we aim to intuitively understand the macroscopic changes in the spray field. By combining previous experimental results, we divided the spray of pressure-swirl nozzle into five regions based on the characteristics of the particle size–velocity distributions of the spray field, namely the mixing, expansion, stabilization, decay, and rarefied regions, as shown in Figure 13. The operating pressure of the nozzle is 2 MPa.

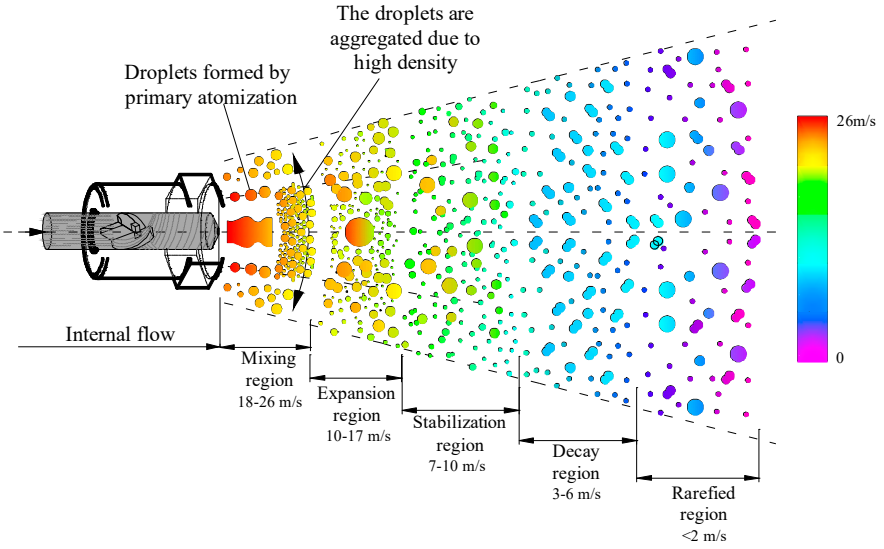

Figure 13. Particle size–velocity spray partition diagram.

(1) Mixing Region (X = 0–100 mm)

Atomization is completed once in this zone. The mixing region is characterized by a high spray density, the droplets do not diffuse in the air, and the droplet velocity and particle size distributions are non-uniform. Furthermore, it is easier for smaller droplets to obtain a higher axial velocity.

(2) Expansion Region (X = 100–400 mm)

Here, the droplets are in a discrete form. Owing to the high relative velocity between the gas and liquid, more droplets undergo atomization for a second time under internal and external forces. As the spray travels forward, it also spreads radially, forming a spray angle. During this process, the velocity is reduced significantly, which is mainly due to air resistance.

(3) Stabilization Region (X = 400–800 mm)

The particles in this region originate from the breakup or cracking of particles in the expansion region and experience great velocity dissipation. This region is characterized by having the most droplets with different sizes that have similar velocities. There are some small droplets that have collided and coalesced, and some high-speed, large droplets that can still break up are present.

(4) Decay Region (X = 800–1000 mm)

In the decay region, the spray concentration decreases and its velocity is extremely low. Here, the droplets are scattered in the air and the interactions between droplets weaken, but the gas–liquid coupling is still strong. The droplets are greatly disturbed by the spray's entrainment, resulting in an increase in the probability of collisions and significantly increasing the number of large droplets. At this point, the interactions between droplets are in the form of "droplet–gas–droplet". Some large droplets continue to break up.

(5) Rarefied Region (spray edge)

This is the outermost region of the spray. Here, the droplets and surrounding air have completed their momentum exchange and their velocities are almost the same. At this point, the droplets are mainly in two forms, i.e., turbulent diffusion and evaporation, and other forms, such as collisions, coalescences, breakups, and spinning, can all be neglected.

3.5. Effect of Water Pressure on Spray Structure

3.5.1. The Effect of Water Pressure on SMD

To present the statistics of SMD on the central axis under 2–5 MPa, the change curves of SMD are shown in Figure 14. When the pressure is 3, 4, and 5 MPa, the changes of SMD are similar. Different from that under 2 MPa, SMD decreases in a wave-like manner when X = 50–400 mm. After X = 800 mm, the SMD remains stable, as opposed to the gradual increase seen under 2 MPa. Moreover, SMD tends to be stable at 450 mm under 2 and 3 MPa. Under 4 MPa, SMD tends to be stable at 350 mm from the nozzle; at 5 MPa, SMD tends to be stable at 100 mm from the nozzle.

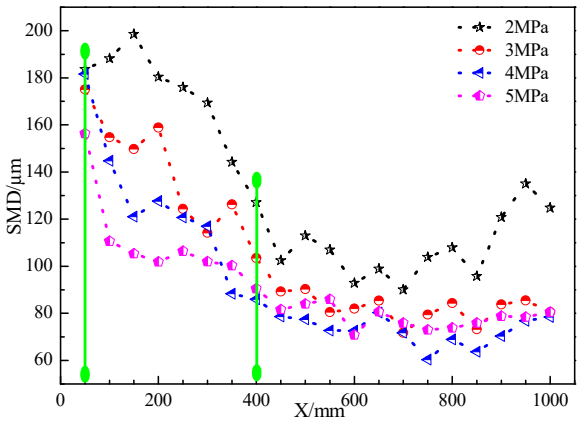

Figure 14. SMD distribution along the central axis at different pressures.

3.5.2. The Effect of Water Pressure on Velocity

Figure 15 shows the change curves of axial and radial velocity. It can be seen that the velocity distribution along the axial direction of the spray is very similar under different pressures. Compared with 2 MPa, the axial velocity increases 1.1 times and the radial velocity increases 6.29 times when X = 600 mm and pressure = 5 MPa. The axial and radial velocity increase 2.65 and 38.5 times, respectively, when X = 1000 mm and pressure = 5 MPa. Thus, the pressure has an obvious effect on the velocity change, and the momentum can still be maintained with the increase of spray distance.

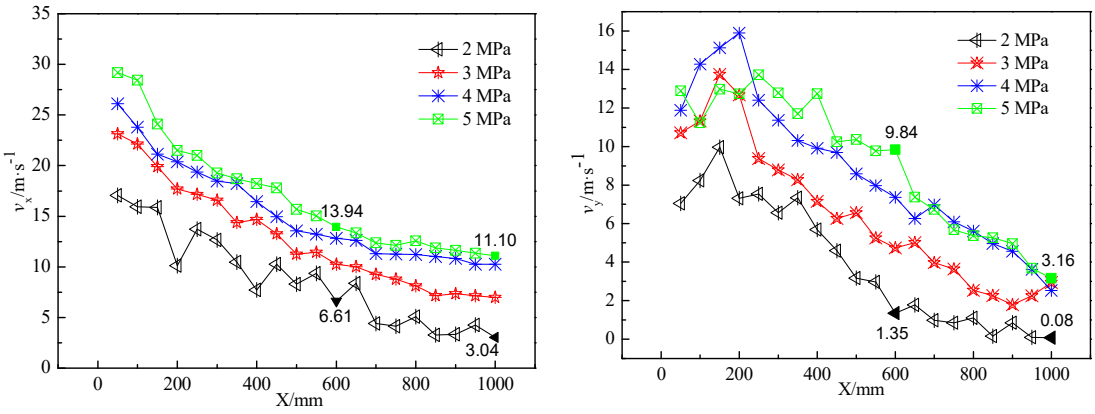

(**a**) axial velocity (**b**) radial velocity

Figure 15. Axial and radial velocity along the axial direction under different pressures.

3.5.3. The Effect of Pressure on the Joint Particle Size–Velocity Distribution Characteristics

Figures 16 and 17 show scatter diagrams of joint particle size–velocity distribution under different pressures at the center points of X = 50 mm and X = 200 mm, respectively. It can be seen from Figure 16 that, as the pressure increases, the velocity of the droplets becomes more and more dispersed. Comparing the SMD under different pressures, it can be found that the particle size distribution of droplets changes little. The main reason for this phenomenon is that the jet breaking is from the outer edge to the core, and the concentration of the spray field near the nozzle is high. At this time, the external air cannot be sucked into the spray field in large quantities to fully mix with droplets, and breakup is not sufficient.

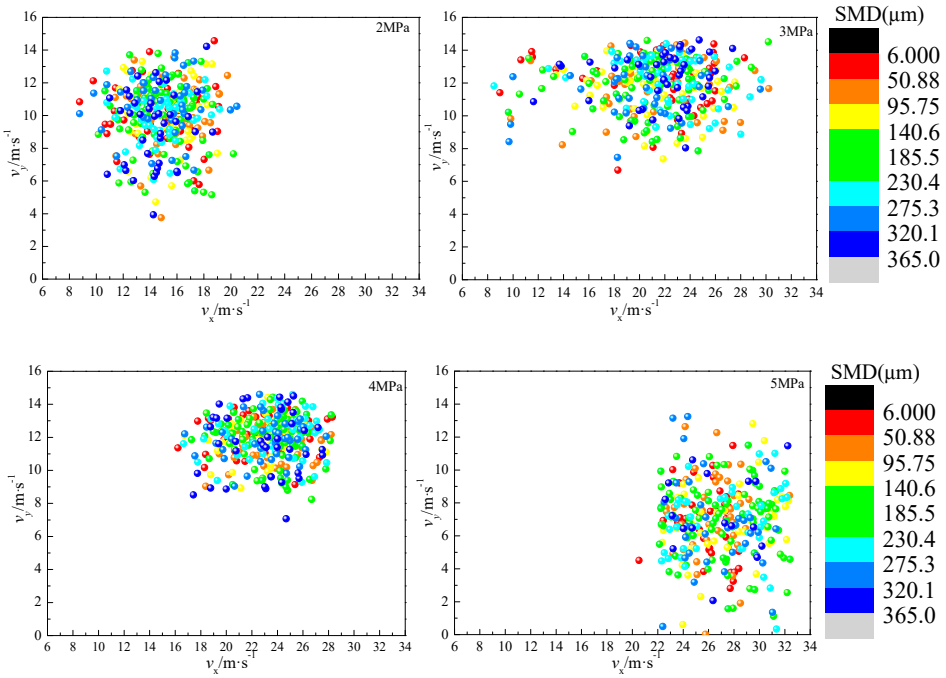

Figure 16. Joint particle size–velocity distribution changes with pressure (X = 50 mm, Y = 0 mm).

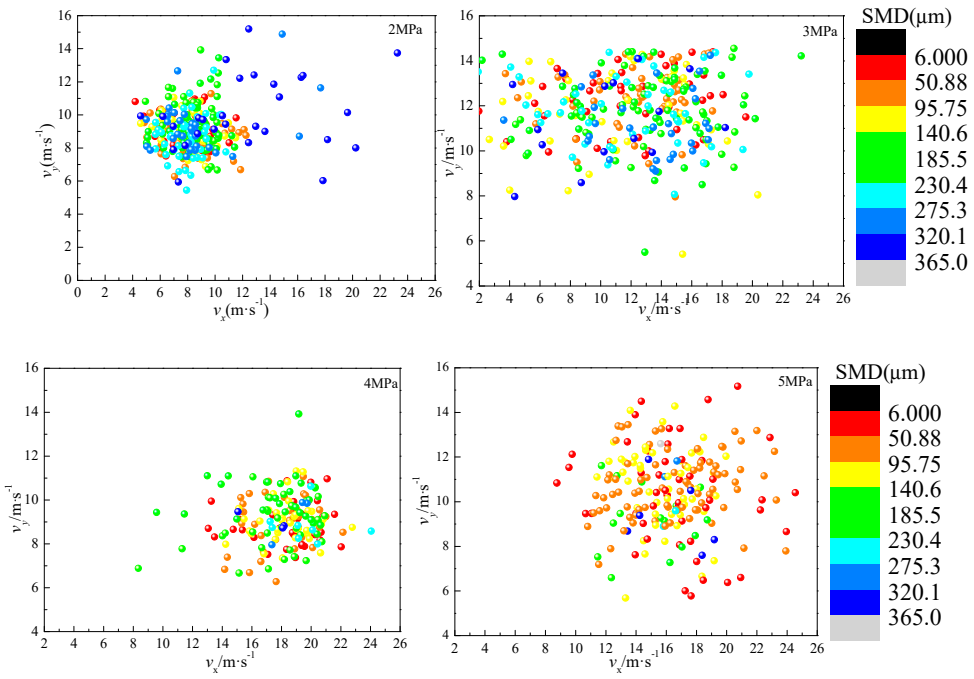

Figure 17. Joint particle size–velocity distribution changes with pressure (X = 200 mm, Y = 0 mm).

According to the previous analysis, when X = 200 mm, the droplet is in the breakup process. Figure 17 shows that with the increase of pressure, the number of droplets with large particle size decreased slowly. When the pressure increased to 4 or 5 MPa, the number of large-size droplets almost disappeared. On the other hand, it reflects that with the increase of pressure, the droplet distribution of the measuring point is more and more uniform. At this time, the droplets still maintain large axial and radial velocities, which shows that the spray field has a strong trend of advance and expansion. When X = 50 mm, with the increase of pressure, the increase of axial velocity slows down obviously, while the trend of droplet size becoming smaller is very obvious, which also verifies that the breakup of droplets is dominant at the moment.

It can be concluded that with the increase of pressure, the spray field structure has two definite characteristics: (1) with the increase of pressure, the expansion region is advanced and the stabilization region becomes larger; (2) with the increase of pressure, the influence of pressure change on SMD decreases for the same measuring point.

The spray dust fall is mainly aimed at dust below 75 μm and the actual spray pressure is above 5 MPa. According to spray partition diagram, when pressure is under 5 MPa, the droplet size in the expansion and stabilization region is about 70–100 μm, and the velocity is between 10 and 25 m/s. In addition, some large-sized droplets will continue to break in the decay region. There are droplets with the sizes close to that of the settling dust in these three regions. Therefore, the expansion, stabilization, and decay regions are the effective dust fall areas of the spray. In addition, the droplet size in the stabilization region is the most uniform, indicating that this region is the best dust-fall region.

4. Conclusions

(1) The variation of SMD in axial and radial directions of the spray has been analyzed. In the axial direction of the spray, when X = 50–150 mm, SMD increases. When X = 150–450 mm, SMD decreases almost by 48.4%. Then, SMD fluctuates between 90 and 110 μm. When x = 800 mm, SMD increases gradually, and the increase rate is 16.0% until the final measurement point (x = 1000 mm). In the radial direction, SMD first increases and then decreases.

(2) The change of velocity in axial and radial directions has been analyzed. In the axial direction of the spray, when X = 50–500 mm, the axial velocity decays rapidly by about 50%, and then the

axial velocity decreases slowly. When X = 50–300 mm, the radial velocity increases by about 10–40%. When x = 300–600 mm, the radial velocity decreases rapidly with an average decrease of 37.9%. Until x = 1000 mm, the radial velocity is maintained at 1–3 m/s. The tangential velocity has no change rule. In the radial direction, axial and radial velocities decrease steadily.

(3) The spray partition frame was determined. Based on the jet atomization theory, the spray structure of pressure-swirl nozzles was divided into five regions, namely the mixing, expansion, stabilization, decay, and rarefied regions. The characteristics of each region are as follows: smaller droplets obtain a larger axial velocity more easily in the mixing region; in the expansion region, the droplet velocity decreases significantly, and the large droplets separate into smaller droplets; in the stabilization region, large droplets have a high velocity and the distributions of the particle size and velocity of the droplets reach a stable state under break-up and collision; in the decay region, the droplet velocity becomes very small, and some large droplets continue to break up under air turbulence; and in the rarefied region, the droplets and surrounding air complete their momentum exchange and reach similar velocities. With the increase of pressure, the expansion region was advanced, the stabilization region became longer. Combined with the above experimental results, the spray field can be further divided for dust control. The expansion, stabilization, and decay regions are the effective dust fall areas and the stabilization region is the best dust fall area.

Author Contributions: J.W.: writing—original draft preparation; C.X.: writing—review and editing; G.Z.: designed the research framework; Y.Z.: Experiment guidance. All authors have read and agreed to the published version of the manuscript.

Funding: Natural Science Foundation of China (5200041899), Natural Science Foundation of Shandong Province (ZR2019MEE118, ZR2019BEE067), Qingdao science and technology plan project (19-3-2-6-zhc).

Conflicts of Interest: The authors declare no conflict of interest.

References

1. Kurnia, J.C.; Sasmito, A.P.; Mujumdar, A.S. Dust dispersion and management in underground mining faces. *Int. J. Min. Sci. Technol.* **2014**, *24*, 39–44. [CrossRef]
2. Prostański, D. Use of Air-and-Water Spraying Systems for Improving Dust Control in Mines. *J. Sustain. Min.* **2013**, *12*, 29–34. [CrossRef]
3. Tessum, M.W.; Raynor, P.C. Effects of Spray Surfactant and Particle Charge on Respirable Coal Dust Capture. *Saf. Health Work.* **2017**, *8*, 296–305. [CrossRef] [PubMed]
4. Walton, W.H.; Woolcock, A. The suppression of airborne dust by water spray. *Int. J. Air Pollut.* **1960**, *3*, 129. [PubMed]
5. Ali, M.; Yan, C.; Sun, Z.; Gu, H.; Mehboob, K. Dust particle removal efficiency of a venturi scrubber. *Ann. Nucl. Energy* **2013**, *54*, 178–183. [CrossRef]
6. Xi, Z.; Jiang, M.; Yang, J.; Tu, X. Experimental study on advantages of foam–sol in coal dust control. *Process. Saf. Environ. Prot.* **2014**, *92*, 637–644. [CrossRef]
7. Pawar, S.K.; Henrikson, F.; Finotello, G.; Padding, J.T.; Deen, N.G.; Jongsma, A.; Innings, F.; Kuipers, J.H. An experimental study of droplet-particle collisions. *Powder Technol.* **2016**, *300*, 157–163. [CrossRef]
8. Azarov, A.; Zhukova, N.; Antonov, F. Water-spray systems reducing negative effects of fine-dispersion dust at operator's workplaces of machine-building industries. *Procedia Eng.* **2017**, *206*, 1407–1414. [CrossRef]
9. Wang, H.; Wang, C.; Wang, D. The influence of forced ventilation airflow on water spray for dust suppression on heading face in underground coal mine. *Powder Technol.* **2017**, *320*, 498–510. [CrossRef]
10. Cheng, L. Collection of Airborne Dust by Water Sprays. *Ind. Eng. Chem. Process. Des. Dev.* **1973**, *12*, 221–225. [CrossRef]
11. Charinpanitkul, T.; Tanthapanichakoon, W. Deterministic model of open-space dust removal system using water spray nozzle: Effects of polydispersity of water droplet and dust particle. *Sep. Purif. Technol.* **2011**, *77*, 382–388. [CrossRef]
12. Tamhane, T.; Joshi, J.; Mudali, K.; Natarajan, R.; Patil, R. Measurement of drop size characteristics in annular centrifugal extractors using phase Doppler particle analyzer (PDPA). *Chem. Eng. Res. Des.* **2012**, *90*, 985–997. [CrossRef]

13. Zhang, Q.; Jamaleddine, T.J.; Briens, C.; Berruti, F.; Hamidi, M.; McMillan, J. Effect of nozzle inclination on jet attrition. *Powder Technol.* **2013**, *241*, 236–243. [CrossRef]
14. Broniarz-Press, L.; Włodarczak, S.; Matuszak, M.; Ochowiak, M.; Idziak, R.; Sobiech, Ł.; Szulc, T.; Skrzypczak, G. The effect of orifice shape and the injection pressure on enhancement of the atomization process for pressure-swirl atomizers. *Crop. Prot.* **2016**, *82*, 65–74. [CrossRef]
15. Jayaraman, N.I.; Jankowski, R.A. Atomization of Water Sprays for Quartz Dust Control. *Appl. Ind. Hyg.* **1988**, *3*, 327–331. [CrossRef]
16. Sun, Y.; Alkhedhair, A.; Guan, Z.; Hooman, K. Numerical and experimental study on the spray characteristics of full-cone pressure swirl atomizers. *Energy* **2018**, *160*, 678–692. [CrossRef]
17. Wang, H.; Wu, J.; Du, Y.; Wang, D. Investigation on the atomization characteristics of a solid-cone spray for dust reduction at low and medium pressures. *Adv. Powder Technol.* **2019**, *30*, 903–910. [CrossRef]
18. Li, Q.; Lin, B.; Zhao, S.; Dai, H. Surface physical properties and its effects on the wetting behaviors of respirable coal mine dust. *Powder Technol.* **2013**, *233*, 137–145. [CrossRef]
19. McCoy, J.F.; Schroeder, W.E.; Rajan, S.R.; Ruggieri, S.K.; Kissell, F.N. New laboratory measurement method for water spray dust control effectiveness. *Am. Ind. Hyg. Assoc. J.* **1985**, *46*, 735–740. [CrossRef]
20. Yu, H.; Cheng, W.; Peng, H.; Xie, Y. An investigation of the nozzle's atomization dust suppression rules in a fully-mechanized excavation face based on the airflow-droplet-dust three-phase coupling model. *Adv. Powder Technol.* **2018**, *29*, 941–956. [CrossRef]
21. Zhang, Q.; Zhou, G.; Qian, X.; Yuan, M.; Sun, Y.; Wang, D.; Yuan, M. Diffuse pollution characteristics of respirable dust in fully-mechanized mining face under various velocities based on CFD investigation. *J. Clean. Prod.* **2018**, *184*, 239–250. [CrossRef]
22. Pollock, D.; Organiscak, J. Airborne Dust Capture and Induced Airflow of Various Spray Nozzle Designs. *Aerosol Sci. Technol.* **2007**, *41*, 711–720. [CrossRef]
23. Kissell, F.N. Handbook for dust control in mining. In *US Department of Health and Human Services*; Public Health Service, Centers for Disease Control and Prevention, National Institute for Occupational Safety and Health: Pittsburgh, PA, USA, 2003.
24. Wang, P.; Tan, X.; Cheng, W.; Guo, G.; Liu, R.; Zhou, G. Dust removal efficiency of high pressure atomization in underground coal mine. *Int. J. Min. Sci. Technol.* **2018**, *28*, 685–690. [CrossRef]
25. Zhang, K.; Zhang, J.; Wei, J.; Ren, T.; Xu, X. Coal seam water infusion for dust control: A technical review. *Environ. Sci. Pollut. Res.* **2019**, *26*, 4537–4554. [CrossRef]
26. O Panão, M.R.; Moreira, A. A real-time assessment of measurement uncertainty in the experimental characterization of sprays. *Meas. Sci. Technol.* **2008**, *19*, 95402. [CrossRef]
27. Mandato, S.; Rondet, E.; Delaplace, G.; Barkouti, A.; Galet, L.; Accart, P.; Ruiz, T.; Cuq, B. Liquids' atomization with two different nozzles: Modeling of the effects of some processing and formulation conditions by dimensional analysis. *Powder Technol.* **2012**, *224*, 323–330. [CrossRef]
28. Jedelsky, J.; Jícha, M. Energy conversion during effervescent atomization. *Fuel* **2013**, *111*, 836–844. [CrossRef]
29. Yu, Y.; Li, G.; Wang, Y.; Ding, J. Modeling the atomization of high-pressure fuel spray by using a new breakup model. *Appl. Math. Model.* **2016**, *40*, 268–283. [CrossRef]
30. Sáenz, J.L.S.; García, J.; Calvo, E.; Cerecedo, L. Effects of droplet collision phenomena on the development of pressure swirl sprays. *Int. J. Multiph. Flow* **2013**, *56*, 160–171. [CrossRef]
31. Husted, B.P.; Petersson, P.; Lund, I.; Holmstedt, G. Comparison of PIV and PDA droplet velocity measurement techniques on two high-pressure water mist nozzles. *Fire Saf. J.* **2009**, *44*, 1030–1045. [CrossRef]
32. Salvador, F.; Romero, J.-V.; Roselló, M.-D.; Jaramillo, D.; Rubio, F.J.S.; Romero, J.-V. Numerical simulation of primary atomization in diesel spray at low injection pressure. *J. Comput. Appl. Math.* **2016**, *291*, 94–102. [CrossRef]
33. Delacourt, E.; Desmet, B.; Besson, B. Characterisation of very high pressure diesel sprays using digital imaging techniques. *Fuel* **2005**, *84*, 859–867. [CrossRef]